Ultrafast Imaging Using Combined Transmissions with Coherence-based Reconstruction

Yang Zhang[1], Yuexin Guo[1], Wei-Ning Lee[1,2]

[1]Department of Electrical and Electronic Engineering, The University of Hong Kong, Hong Kong.
[2]Medical Engineering Programme, The University of Hong Kong, Hong Kong.

Abstract— **Ultrafast plane wave (PW) imaging and synthetic aperture (SA) imaging have become the prevalent techniques for non-conventional medical ultrasound imaging. In both imaging techniques, the image contrast is generally compromised by reducing the number of transmissions for high frame rate. Moreover, the axial ghost artifact in PW imaging has been demonstrated attributed to the edge array elements. We hereby propose a new methodology that achieves high contrast and reduces the axial ghost artifact with only three transmissions for ultrafast imaging. A new coherence-based factor was derived. The raw data from the PW and the spherical wave (SW) transmissions were compounded based on the factor, with the consideration of their respective coherence and interrelationship, to suppress the side lobes and reduce the axial artifact. Field II simulations show that our proposed method greatly reduced the axial artifact by 20 dB ~ 35 dB compared with coherent plane wave compounding (CPW) and suppressed side lobes by 15 dB ~ 30 dB compared with CPW and sparse SA imaging.**

Keywords— Ultrafast imaging; Combined transmissions; Coherence-based reconstruction

I. INTRODUCTION

Ultrafast ultrasound imaging, which can achieve a frame rate on the order of kHz, plays an increasingly important role in noninvasive measurement of tissue function and properties for clinical diagnosis [1]. It enables much better measurement than conventional focused ultrasound imaging of tissue motion, blood motion, contrast agent dynamics, and even neurovascular coupling. For example, ultrasound imaging with a frame rate on the order of kHz gives access to imaging of natural waves and shear wave elastography. Ultrafast Doppler imaging can be implemented to provide a full 2-D map of the blood flow. Also, an improved contrast imaging and information about tissue properties can be obtained by ultrafast contrast imaging.

One method to obtain ultrafast images is plane wave imaging, in which planar wavefront is transmitted by activating the array elements simultaneously, and the backscattered signals are collected by the full aperture of the same array probe to reconstruct an image. The development of plane wave imaging consists of a time reversal approach, parallel processing technique, limited diffraction beams and coherent plane wave compounding. The time-reversal approach was proposed by Fink et al. to implement parallel processing [2] for the formation of a full-view image from a single acoustic pulse. Lately, plane-wave illuminations with parallel receive beamforming was demonstrated capable of achieving ultrafast imaging with a frame rate higher than 1 kHz [3]. Another approach for achieving high frame rates was proposed by Lu and Greenleaf in the 1990s with a plane wave pulse transmission and limited diffraction beams [4, 5]. Recently, a significant advancement was the development of coherent compounding in the plane wave imaging technology, coined as coherent plane wave compounding (CPW), for high frame-rate (> 1 kHz) ultrasonography and transient elastography [6] in 2009. The coherent summation of beamformed radio frequency (RF) data, obtained by plane wave transmissions with different angles, led to equivalent image quality to that of conventional multi-focus ultrasound imaging.

Meanwhile, another significant method named synthetic aperture (SA) imaging was applied to medical ultrasound imaging by Jensen in 2006 [7]. In contrast to the plane wave transmission, spherical wave was transmitted sequentially from each array element, and for each transmission, full aperture was used on receive to generate a low-resolution beamformed RF image. A final high-resolution image was obtained by compounding all the low-resolution images.

Although PW and SA imaging are the most prevalent techniques for non-conventional ultrasound imaging, they both have some drawbacks. In PW imaging, since there is no real transmit focus for single or several angles, the clutters will not be successfully suppressed compared with optimal multi-focusing. Thus, both the axial ghost artifact mentioned in [8] and the side lobes lead to low image contrast. In SA imaging, the SNRs and the frame rate may be lowered, and the capability of the suppression of clutters is determined by the number of transmissions. Overall, the image contrast is traded for high frame rates in ultrafast imaging.

Several techniques have been investigated to overcome the drawbacks of PW and SA imaging. In PW imaging, apodization techniques have been demonstrated to reduce the axial ghost artifact. One is the integrated transmit apodization suggested by Jensen et al for single plane wave transmission in row-column array [8]. Another is the angular apodization for coherent plane wave compounding [9]. The transmit apodization used in the conventional ultrasound imaging was applied as angular apodization in PW imaging but defined over the entire angle sequence. However, the transmit apodization method leads to the change of wavefront and lowed signal energy, and the angular apodization requires multiple angle plane wave transmissions. In order to improve the frame rate and SNR of conventional SA imaging, sparse synthetic aperture imaging and diverging wave transmission techniques were developed respectively. The use of sparse distribution of single transmit

elements of the array was simulated for real-time 3-D imaging [10] to increase the frame rate. Recently, diverging wave transmissions, where virtual sources were placed behind the array, have been realized for high contrast cardiac imaging with high SNR and frame rates (e.g., 2500 frames/s using 5 diverging waves) [11]. In addition, a first attempt of combing the individual benefits of PW and SA imaging was made by Kotowick et al. in 2013 [12]. The adaptive combination of 64-transmit PW and 64-transmit SA imaging was demonstrated to improve the spatial resolution over PW and signal-to-noise ratio over SA at half the standard number of transmits. However, the aforementioned combined techniques are not shown capable of suppressing the axial ghost artifacts and side lobes.

Inspired by [8] and [12], we hereby propose a new methodology with only three transmissions for ultrafast imaging. The signals from the PW and the spherical wave (SW) transmissions are both utilized to suppress the side lobes and reduce the axial ghost artifact for the improvement of image contrast. In our method, three transmissions are used with one PW transmitted by full aperture and two SWs transmitted respectively by the leftmost and the rightmost array elements. Full aperture was used on receive for each transmission. To balance between the frame rate and image contrast, we have derived a cross coherence factor, taking into account the coherence of single aperture and the coherence between each pair of aperture data.

II. Materials and Methods

The aim of this work is to combine PW and SW transmissions and to design a reconstruction method to improve the image quality for ultrafast imaging. The diagram of our proposed method is shown in Fig. 1. Three transmissions were realized with one PW transmitted by full aperture and two SWs transmitted respectively by the leftmost and rightmost array elements. Full aperture was used on receive for each transmission. Firstly, the channel data from PW transmission was preprocessed to reduce the echoes which caused the axial ghost artifact in the point spread function. Secondly, three aperture data for each image pixel to be reconstructed were obtained from the three transmissions. Then cross-coherence factors were designed based on the three aperture data. Finally, the mean value of each aperture data was weighted by the
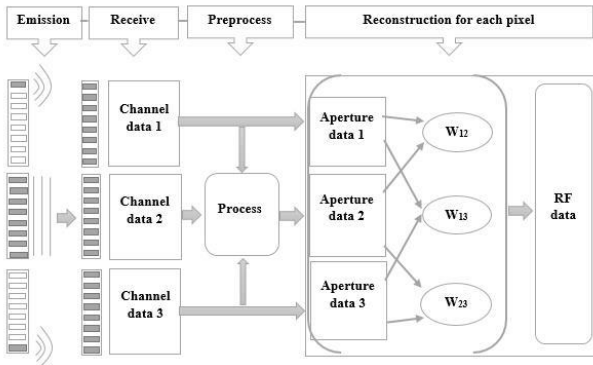

Fig. 1. Diagram of proposed method

designed coefficient and then summed to obtain the radio frequency (RF) signal for each pixel.

A. Field II simulation

An L7-4 linear array probe of 128 elements with 0.3-mm pitch and a center frequency of 5.2-MHz (100% bandwidth) was simulated in Field II [13]. The sampling frequency of backscattered signals was 100 MHz. Both point targets and vessel phantom were simulated. Five point targets were equally spaced from 20 mm to 50 mm in depth. For vessel phantom, both top wall and bottom wall were 2 mm thickness. Point scatterers were randomly distributed in the vessel wall, with the scattering amplitude following a Gaussian distribution.

B. Axial ghost artifact

One drawback of plane wave imaging is the apparent axial ghost artifact in the point spread function caused by edge waves. Such edge effect was first investigated by theoretically analyzing the spatial impulse response of line elements [8]. It was demonstrated to be caused by the discontinuity of apodization at the element edges. Based on their work of line elements, we used Field II to simulate and analyze the location and amplitude of axial ghost artifact in plane wave imaging.

Point spread function: Single plane wave with 0 degree was transmitted to obtain the point spread function in Fig. 2. One axial ghost artifact appears below a real point target at (0, 40) mm, and two separated axial ghost artifacts are present below a real point target at (-5, 40) mm. Based on the geometrical relationship among the array, the point target, and axial ghost artifact, we found that the distance between the artifact and the point target was half the differential distance between edge elements and their nearest elements.

Ghost echoes: The amplitudes and phases of the ghost echoes by PW are compared with those of the backscattered signals by SW as shown in Fig. 3. The phase of the channel data from SW transmission was found to equate that of the ghost echoes from PW transmission. The normalized backscattered signal amplitude of two SWs was also comparable to that of the PW transmission.

Preprocess: We therefore reduced the ghost artifact by designing a preprocess procedure as follows: (1) Find the zero-crossing points of channel data of the PW transmission. (2) Calculate the cross-correlation coefficients between two channel data obtained by PW and SW transmission.(3) Suppress
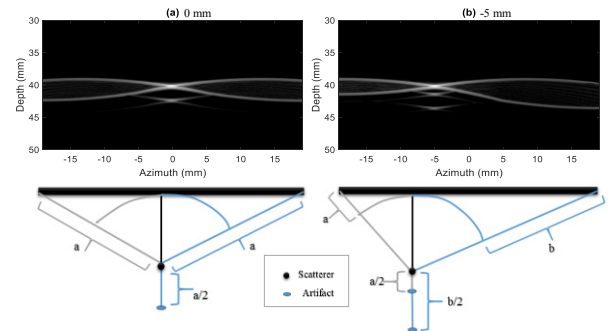

Fig. 2. Point spread function and location of axial ghost artifacts of plane wave imaging at (a) 0 mm and (b) -5 mm with 60 dB dynamic range.

[14] the selected segments of channel data with high correlation coefficients and small amplitude differences without changing the phases.

C. Side lobe suppression

To evaluate the coherence among three aperture data, we derived a new factor from the conventional coherence factor [15, 16] and the Tanimoto coefficient [17]. For the conventional coherence factor, only one aperture data was considered. Our new derived factor considered both the property of one aperture data and the mutual relationship of the three aperture data. Tanimoto coefficient is used to measure the similarity and diversity of data sets. It is

$$c_0 = \frac{\sum_i x_i y_i}{\sum_i x_i^2 + \sum_i y_i^2 - \sum_i x_i y_i}. \tag{1}$$

To consider all the combinations of samples in two aperture data, we revised the formula as

$$c'_{xy} = \frac{\sum_i \sum_j x_i y_j}{N(\sum_i x_i^2 + \sum_j y_j^2) - \sum_i \sum_j x_i y_j}, \tag{2}$$

where N is the number of samples. Compatible with the conventional coherence factor, it can be simplified and modified as

$$c_{xy} = \frac{\mu_x \mu_y}{\mu_x^2 + \mu_y^2 - \mu_x \mu_y + (\sigma_x^2 + \sigma_y^2)/2}, \tag{3}$$

where μ_x and μ_y are the mean values, and σ_x and σ_y are the standard deviations. When the two aperture data are the same, this factor is equivalent to the conventional coherence factor. Since we have three aperture data, three factors can be obtained from each pair. We can write a matrix as

$$r = \begin{bmatrix} 1 & c_{12} & c_{13} \\ c_{21} & 1 & c_{23} \\ c_{31} & c_{32} & 1 \end{bmatrix}. \tag{4}$$

Then, the final coefficient can be obtained by

$$C = \sqrt{1 - \det(r)}. \tag{5}$$

Finally, the square root of the derived coefficient is used as the multiplex factor for the sum of the respective averages of the three aperture data,

$$Rf(x, y) = \sqrt{C} \cdot (A_1 + A_2 + A_3), \tag{6}$$

where A_1, A_2, and A_3 are the respective averages of the three aperture data.

III. RESULTS

Fig. 4 shows the B-mode images of point targets. Both axial ghost artifacts and side lobes were observed in single plane wave imaging and coherent plane wave compounding. Only side lobes were noted in single and three spherical wave imaging. Both axial ghost artifacts and side lobes were present in that by coherent summation of plane wave and two spherical waves. The axial ghost artifacts were reduced by our proposed preprocess procedure for single plane wave, and the side lobes were reduced by simply employing coherence-based reconstruction. Our proposed method, comprised of both preprocess and coherence-based reconstruction, was demonstrated to greatly reduce both axial ghost artifacts and side lobes.

Fig. 5 shows the B mode images of a simulated vessel phantom. Both axial ghost artifacts and side lobes were pronounced in the lumen of the vessel phantom as shown in Figs. 13(a)-(e). Artifacts were again removed in the lumen of the vessel phantom by the proposed method (Fig. 13(f)).

Fig. 6 shows the profiles of point targets and the simulated vessel phantom. The axial and lateral profiles of the PSFs shown in Figs. 6(a)-(b) demonstrated that our proposed method greatly reduced the axial artifact by 20 dB ~ 35 dB compared with
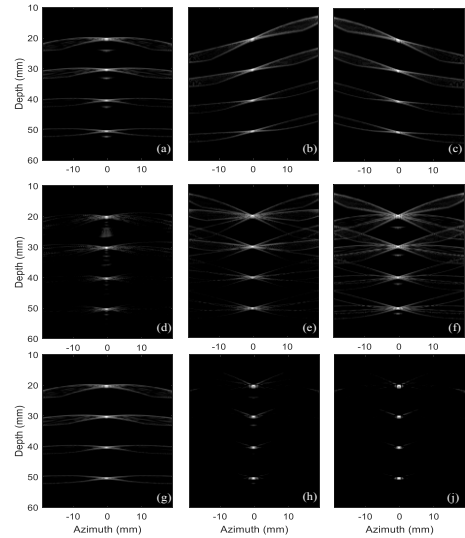
Fig.4. B-mode images of four point targets with a 50 dB dynamic range. (a) 1 plane wave at 0 degree, (b) 1 spherical wave by the leftmost element, (c) 1 spherical wave by the rightmost element, (d) 3 plane waves with coherent compounding at -14 degrees, 0 degree, and 14 degrees, (e) 3 spherical waves with coherent compounding by the leftmost, middle and rightmost elements, (f) 1 plane wave and two spherical waves, (g) 1 plane wave with preprocess, (h) combined transmissions without preprocess (f) proposed method with combined transmissions.
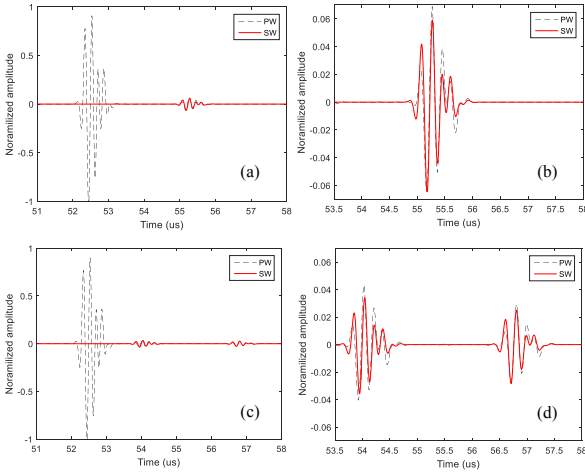

Fig. 3. Chanel data of point targets by PW and SW transmissions: (a) and (b) a point target at (0, 40 mm), (c) and (d) a point target at (-5 mm, 40 mm).
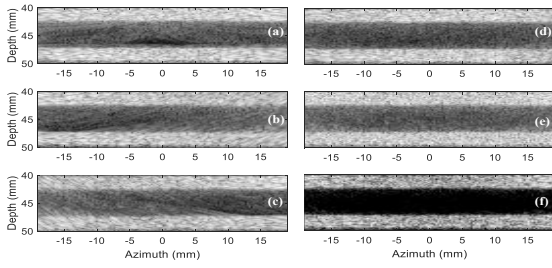
Fig.5. B-mode images of a simulated vessel phantom with a 60 dB dynamic range. (a) 1 plane wave at 0 degree, (b) 1 spherical wave by the leftmost element, (c) 1 spherical wave by the rightmost element, (d) 3 plane waves with coherent compounding at -14 degrees, 0 degree, and 14 degrees, (e) 3 spherical waves with coherent compounding by the leftmost, middle and rightmost elements, (f) proposed method with combined transmissions.
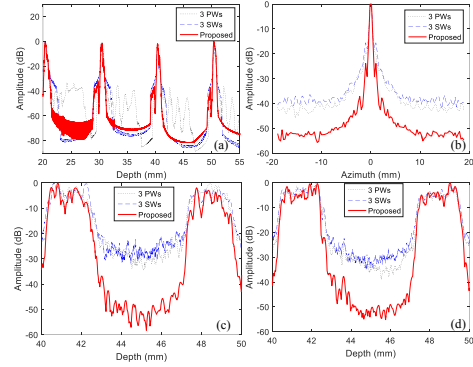

Fig. 6. (a) Axial profile and (b) lateral profile of the point targets at 50 mm in depth. And axial profile of the vessel phantom: (c) Left side of vessel wall with azimuth from -18.9 mm to -15.0 mm, (d) middle of vessel wall with azimuth from -2.8 mm to 2.8 mm.

coherent plane wave compounding (CPW) and suppressed side lobes by approximately 15 dB compared with CPW and SW imaging. Figs. 6(c) (d) show the profiles on the left side and in the middle of the simulated vessel phantom. The reduction of artifacts in the lumen of the vessel phantom was found to be 25 dB ~ 30 dB by the proposed method.

IV. DISCUSSION AND CONCLUSION

In this paper, ultrafast imaging using combined PW and SW transmissions with coherence-based reconstruction was proposed to reduce both the axial ghost artifact and side lobes. Field II simulations revealed the location and amplitude of ghost echoes in backscattered signals by PW illumination, and our proposed preprocess method could reduce the axial ghost artifacts in PW imaging. In addition, to overcome the tradeoff of the frame rate and image contrast, a new cross-coherence factor was derived to suppress the side lobes in ultrafast imaging.

In conclusion, we demonstrated the feasibility of the combined PW and SW transmissions with cross coherence-based reconstruction in reducing the axial ghost artifact and side lobes in ultrafast imaging. Based on the analysis of axial artifacts and side lobes, proposed method reduce the axial artifacts by 20dB ~ 35 dB, and suppress the side lobes 15dB ~ 30dB.

One of the limitations of this work is the weak energy of the SW transmissions by the leftmost and rightmost elements. Since only one element was used to generate a SW, the signal would be affected by the noise in the deep region of interest in the scanned medium. Future work consists in replacing the SW transmissions by diverging wave transmissions.

REFERENCES

[1] M. Tanter and M. Fink, "Ultrafast imaging in biomedical ultrasound," *IEEE transactions on ultrasonics, ferroelectrics, and frequency control,* vol. 61, pp. 102-119, 2014.

[2] M. Fink, "Ultrasound imaging," *REVUE DE PHYSIQUE APPLIQUEE,* vol. 18, pp. 527-556, 1983.

[3] L. Sandrin, S. Catheline, M. Tanter, X. Hennequin, and M. Fink, "Time-resolved pulsed elastography with ultrafast ultrasonic imaging," *Ultrasonic imaging,* vol. 21, pp. 259-272, 1999.

[4] J.-y. Lu and J. F. Greenleaf, "Pulse-echo imaging using a nondiffracting beam transducer," *Ultrasound in medicine & biology,* vol. 17, pp. 265-281, 1991.

[5] J.-y. Lu, "2D and 3D high frame rate imaging with limited diffraction beams," *IEEE transactions on ultrasonics, ferroelectrics, and frequency control,* vol. 44, pp. 839-856, 1997.

[6] G. Montaldo, M. Tanter, J. Bercoff, N. Benech, and M. Fink, "Coherent plane-wave compounding for very high frame rate ultrasonography and transient elastography," *IEEE transactions on ultrasonics, ferroelectrics, and frequency control,* vol. 56, pp. 489-506, 2009.

[7] J. A. Jensen, S. I. Nikolov, K. L. Gammelmark, and M. H. Pedersen, "Synthetic aperture ultrasound imaging," *Ultrasonics,* vol. 44, pp. e5-e15, 2006.

[8] T. L. Christiansen, M. F. Rasmussen, J. P. Bagge, L. N. Moesner, J. A. Jensen, and E. V. Thomsen, "3-D imaging using row column-addressed arrays with integrated apodization part ii: transducer fabrication and experimental results," *IEEE transactions on ultrasonics, ferroelectrics, and frequency control,* vol. 62, pp. 959-971, 2015.

[9] A. Rodriguez-Molares, H. Torp, B. Denarie, and L. Løvstakken, "The angular apodization in coherent plane-wave compounding [Correspondence]," *IEEE transactions on ultrasonics, ferroelectrics, and frequency control,* vol. 62, pp. 2018-2023, 2015.

[10] G. R. Lockwood, J. R. Talman, and S. S. Brunke, "Real-time 3-D ultrasound imaging using sparse synthetic aperture beamforming," *IEEE transactions on ultrasonics, ferroelectrics, and frequency control,* vol. 45, pp. 980-988, 1998.

[11] C. Papadacci, M. Pernot, M. Couade, M. Fink, and M. Tanter, "High-contrast ultrafast imaging of heart," *IEEE transactions on ultrasonics, ferroelectrics, and frequency control,* vol. 61, pp. 288-301, 2014.

[12] K. Kotowick, R. Rohling, and L. Lampe, "Adaptive compounding of synthetic aperture and compounded plane-wave imaging for fast ultrasonography," in *2013 IEEE 10th International Symposium on Biomedical Imaging*, 2013, pp. 784-787.

[13] J. A. Jensen, "Field: A program for simulating ultrasound systems," in *10TH NORDICBALTIC CONFERENCE ON BIOMEDICAL IMAGING, VOL. 4, SUPPLEMENT 1, PART 1: 351--353*, 1996.

[14] C. H. Seo and J. T. Yen, "Sidelobe suppression in ultrasound imaging using dual apodization with cross-correlation," *IEEE transactions on ultrasonics, ferroelectrics, and frequency control,* vol. 55, pp. 2198-2210, 2008.

[15] K. Hollman, K. Rigby, and M. O'Donnell, "Coherence factor of speckle from a multi-row probe," in *Ultrasonics Symposium, 1999. Proceedings. 1999 IEEE*, 1999, pp. 1257-1260.

[16] P.-C. Li and M.-L. Li, "Adaptive imaging using the generalized coherence factor," *IEEE transactions on ultrasonics, ferroelectrics, and frequency control,* vol. 50, pp. 128-141, 2003.

[17] D. Bajusz, A. Rácz, and K. Héberger, "Why is Tanimoto index an appropriate choice for fingerprint-based similarity calculations?," *Journal of cheminformatics,* vol. 7, p. 1, 2015.